第 43 卷 第 9 期/2023 年 5 月/光学学报 研究论文

光学学报

基于R-C耦合跨阻设计的1 kHz~200 MHz宽带平衡零拍探测器

王少锋[1,2**]，刘宣泽[2]，李汉卿[2]，李康康[2]，董瑞芳[1*]

[1]中国科学院国家授时中心时间频率基准重点实验室，陕西 西安 710600；

[2]山西大学物理电子工程学院，山西 太原 030006

摘要 通过分析平衡零拍探测器的噪声来源，采用电阻-电容(R-C)耦合跨阻电路方案并优化跨阻放大电路结构，实现了一种低噪声、高共模抑制比的宽带平衡零拍探测器，工作带宽为1 kHz~200 MHz。当光功率为8 mW的1550 nm激光入射时：在5 kHz分析频率处散粒噪声功率比电子学噪声功率高12 dB，共模抑制比达到70 dB；在100 MHz分析频率处散粒噪声功率比电子学噪声功率高20 dB，共模抑制比达到66 dB。该探测器可以为低频引力波探测、高速连续变量量子密钥分发和高速量子随机数发生器等应用提供高性能的探测工具。

关键词 光学器件；跨阻放大器；散粒噪声；共模抑制比；信噪比；电子学噪声

中图分类号 O431.2 **文献标志码** A **DOI**：10.3788/AOS221746

1 引 言

平衡零拍探测器(BHD)[1]对入射光振幅、相位有着很高的敏感性，用于可靠地提取量子态正交分量的噪声起伏，具有将经典共模噪声抑制的同时还能将量子正交分量起伏放大到宏观水平的特性[2-3]，目前已被广泛应用于量子噪声测量、引力波探测、高灵敏时延抖动测量、连续变量量子密钥分发和量子随机数发生器等领域中[4-13]。

探测器的带宽、信噪比和共模噪声抑制比等性能决定了平衡零拍探测系统的应用极限，探测器的优化设计一直是研究热点。2010年，周倩倩等[14]设计了一种用于量子光学实验中量子噪声测量的低噪声光电探测器，2~31 MHz分析频率内共模抑制比高于30 dB，2~50 MHz分析频率内4 mW入射光功率下信噪比高于10 dB。2012年，Kumar等[15]设计了一种多功能宽带平衡零拍探测器，该探测器带宽为100 MHz，12 mW入射光功率下信噪比为13 dB，共模抑制比为52.4 dB。2013年，Huang等[16]设计了一种高速平衡零拍探测器，该探测器带宽为300 MHz，6.13 mW入射光功率下信噪比高于14 dB，共模抑制比为54 dB。2018年，Zhang等[17]设计出了带宽为1.2 GHz的平衡零拍探测器，10.05 mW入射功率下其信噪比约为18 dB，共模抑制比为57.9 dB。2020年，Wang等[18]设计了低频高信噪比的平衡零拍探测器，在1~100 kHz分析频率内，8 mW入射功率下最大信噪比为48 dB，共模抑制比高于59 dB。

在平衡零拍探测过程中，信号光与本地光在50/50分束器(BS)上发生干涉，分束器输出两臂入射到探测器的光电二极管(PD)中，然后对光电流信号进行减法和放大处理。基于直流(DC)耦合的跨阻放大电路并不适用于量子噪声的探测[5]。随着入射光强的增加，不平衡的直流电流迅速增大，从而使跨阻运放饱和，这将显著降低探测器的动态响应范围。由于电感的寄生效应和电感在低频时的低阻抗特性，基于电感-电容(L-C)耦合电路的平衡零拍探测器[19]在千赫兹量级分析频率处存在较高的电子学噪声，并不适合低频测量。本文采用电阻-电容(R-C)耦合跨阻放大电路实现了千赫兹分析频率的平衡零拍测量，理论分析了平衡零拍探测器的噪声来源，同时优化跨阻放大电路结构将工作带宽提高到了200 MHz。通过光电流“自减”设计、分束器分束比的精密调节和可调反向偏压设计[20-22]，探测器的共模抑制比得到了提高。该探测器可为低频引力波探测、高速连续变量量子密钥分发和高速量子随机数发生器等应用提供高性能的探测工具。

收稿日期：2022-09-26；**修回日期**：2022-11-23；**录用日期**：2022-12-02；**网络首发日期**：2023-01-04

基金项目：国家自然科学基金(61875205，12033007)、中国科学院时间频率基准重点实验室开放基金、山西省高等学校科技创新项目(2020L0034)

通信作者：*dongruifang@ntsc.ac.cn；**wangshaofeng@sxu.edu.cn

2　基于R-C耦合跨阻设计的平衡零拍探测器的结构原理

2.1　探测器电路结构

图1是基于R-C耦合跨阻设计的平衡零拍探测器电路原理图，其中C_f是跨阻放大器的反馈电容，R_f是反馈电阻。PD1、PD2是串联连接的两个光电二极管，将串联节点处的光电流信号经过R-C耦合结构分成直流信号(DCS)和交流(AC)信号(ACS)，频率拐点为$1/(2\pi CR_{DC})$，其中C为耦合电容。交流信号通过跨阻放大器(TIA)转换成电压信号进行放大，用于衡量入射激光的散粒噪声强度。直流信号经过负载电阻R_{DC}后产生电压，用于衡量两束入射光的平衡程度。为了降低直流端对交流端的噪声串扰，在R_{DC}之后加入隔离放大器。可调反向偏置电压(V_B)用于调节光电二极管的结电容，提高探测器共模抑制比。

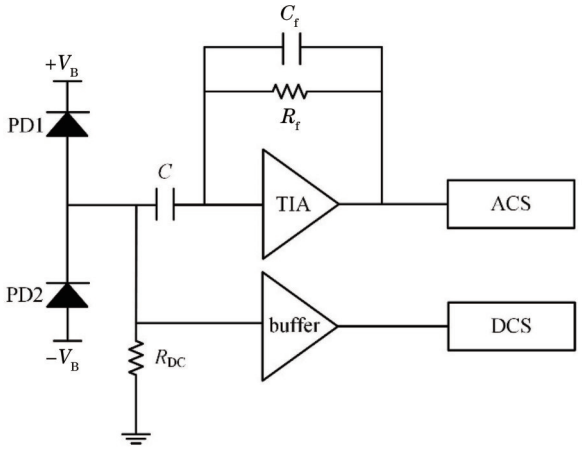

图1　1 kHz～200 MHz宽带平衡零拍探测器的电路原理图

Fig. 1　Circuit schematic diagram of 1 kHz-200 MHz broadband balanced homodyne detector

2.2　探测器噪声分析

图2是平衡零拍探测器等效噪声模型[23-25]。注入激光后光电二极管产生的光电流分别为i_{d1}和i_{d2}。受到光电二极管暗电流、反馈电阻热噪声、印刷电路板(PCB)杂散电容和放大器电子学噪声等影响，探测器的交流输出端除了信号外还混杂有复杂的电子学噪声，而过量的电子学噪声会引起信号失真。

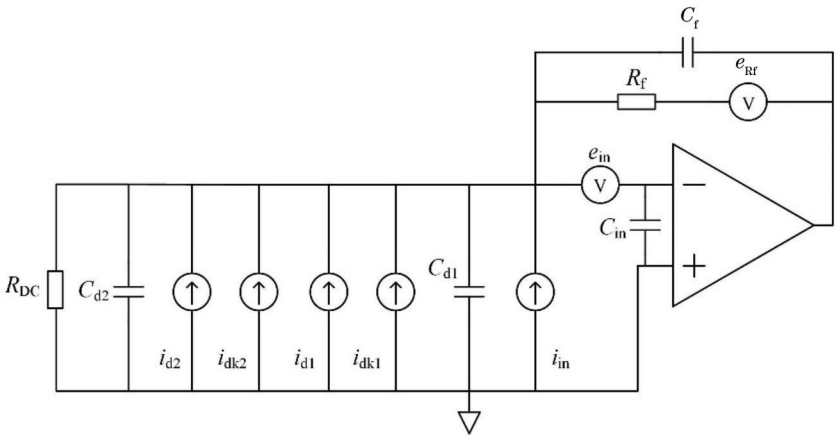

图2　平衡零拍探测器等效噪声模型

Fig. 2　Equivalent noise model of balanced homodyne detector

平衡零拍探测器的电子学噪声主要源于4部分：光电二极管暗电流引入的噪声e_{PD1}和e_{PD2}、跨阻放大电路中反馈电阻的热噪声e_{Rf}、跨阻放大器输入电流噪声产生的噪声$e_{TIA\text{-}current}$和跨阻放大器输入电压噪声产生的噪声$e_{TIA\text{-}voltage}$。两个光电二极管暗电流引入的噪声可以分别表示为

$$e_{PD1}=\sqrt{2qi_{dk1}}\times|Z_s|, \tag{1}$$

$$e_{PD2}=\sqrt{2qi_{dk2}}\times|Z_s|, \tag{2}$$

式中：i_{dk1}和i_{dk2}为两个光电二极管的暗电流；q是电子电量；Z_s是跨阻放大电路的增益阻抗，其表达式为

$$Z_s=\frac{R_f}{1+j2\pi fC_fR_f}, \tag{3}$$

式中：f为分析频率。

跨阻放大电路中反馈电阻的热噪声为

$$e_{Rf}=\sqrt{\frac{4kT}{R_f}}\times|Z_s|, \tag{4}$$

式中：k为玻尔兹曼常数；T为绝对温度。

跨阻放大器的输入电流噪声i_{in}本质上是放大器输入端偏置电流的散粒噪声，其引起的噪声输出为

$$e_{TIA\text{-}current}=i_{in}\times|Z_s|, \tag{5}$$

跨阻放大器的输入电压噪声e_{in}引起的噪声输出为

$$e_{TIA\text{-}voltage}=e_{in}\times|Z_o|, \tag{6}$$

式中：Z_o是跨阻放大器的电压噪声增益，可以表示为

$$Z_o=\frac{Z_d+Z_s}{Z_d}, \tag{7}$$

$$\begin{cases}Z_d=\dfrac{R_{DC}}{1+j2\pi fC_dR_{DC}}\\ C_d=C_{d1}+C_{d2}+C_{in}\end{cases}, \tag{8}$$

式中：C_{d1}和C_{d2}分别是两个光电二极管的结电容；C_{in}是跨阻放大器的输入电容，它包括共模输入电容和差模输入电容两部分；R_{DC}是直流端负载电阻。由此可见，光电二极管的结电容、放大器的输入电容、反馈电容和直流负载都会对输入电压噪声e_{in}的增益产生影响，从而影响探测器的电子学噪声。

综合式(1)～(8)，上述4种噪声共同组成了放大器的电子学噪声。4种噪声互不相关，平衡零拍探测器的总电子噪声可以表示为

$$e_{ele}=\sqrt{e_{PD1}^2+e_{PD2}^2+e_{Rf}^2+e_{TIA\text{-}current}^2+e_{TIA\text{-}voltage}^2}。\quad(9)$$

通过噪声分析可知，合理设置直流负载电阻R_{DC}和反馈电容C_f并选择低暗电流、低结电容的光电二极管和低输入噪声的跨阻放大器可以降低探测器的电子学噪声，从而提高探测器信噪比。

3　实验结果

探测器选用北京敏光科技有限公司的LSIPD-LD50光纤型光电二极管，该二极管在反向偏置电压为−5 V时，暗电流非常微弱(5 pA)，故暗电流产生的噪声可以忽略。此时，3 dB带宽为3 GHz，结电容为0.8 pF。跨阻放大器选用TEXAS INSTRUMENTS公司生产的OPA855，该放大器具有8 GHz的增益带宽积，输入电压噪声为0.98 nV·Hz$^{-1/2}$，输入电流噪声为2.5 pA·Hz$^{-1/2}$，输入电容为0.8 pF。直流负载电阻设置为1 kΩ。反馈电容可以使跨阻放大器处于稳定的工作状态，但电路板杂散电容和反馈电阻的寄生电容会使得反馈电容偏大，进而降低了探测器的带宽。去除跨阻放大器周围的接地铜箔，选用低寄生电容的电阻和减少反馈电阻与跨阻放大器之间的PCB走线长度可以提高带宽。最终，反馈电容为0.2 pF，反馈电阻为10 kΩ。

为测试平衡零拍探测器的性能，搭建了测试装置，如图3所示。波长为1550 nm的光纤激光器作为入射光源，通过衰减器对入射光功率进行调节。在衰减器和光学分束器之间加入电光振幅调制器(EOAM)，信号发生器(SG)产生的调制信号通过电光振幅调制器对入射光的强度噪声进行调制，用于测量探测器的共模抑制比。入射激光接入50/50光学分束器后，两束光分别被平衡零拍探测器的两个光电二极管探测到，产生的两束光电流进行减法处理后经过R-C耦合结构被分成直流和交流两路信号。交流信号通过频谱分析仪(SA，是德科技，N9010A)后，可测量得到平衡零拍探测器的工作带宽和信噪比。直流信号进入示波器(OSC)后，可测量得到两束光的平衡程度。

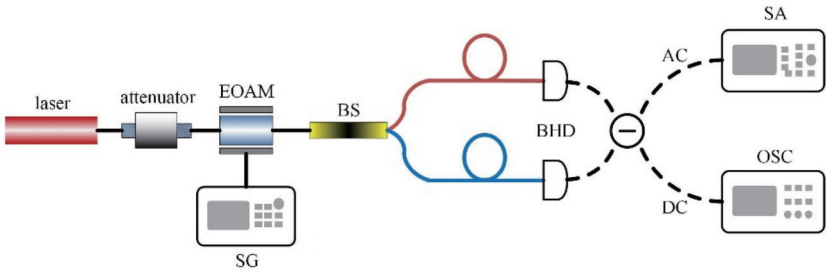

图3　平衡零拍探测器测试装置图

Fig. 3　Test devices of balanced homodyne detector

当入射光功率分别为8、4、2、1 mW时，平衡零拍探测器在不同工作频段的散粒噪声功率、电子学噪声功率和频谱仪背景噪声功率测试结果如图4所示。测试结果表明：平衡零拍探测器的3 dB工作带宽为1 kHz～200 MHz。在图4(a)中，频谱分析仪的分辨率带宽(RBW)为10 Hz、视频带宽(VBW)为1 Hz，平均次数(AVG)设为40，入射光功率为8 mW时5 kHz分析频率处散粒噪声功率比电子学噪声功率高12 dB，即探测器的信噪比为12 dB。随着分析频率的升高，1/f噪声下降导致探测器总的电子学噪声下降，信噪比升高。在图4(b)中，RBW为200 kHz，VBW为100 Hz，在100 MHz分析频率处的信噪比为20 dB。同时，图4表明，在10 kHz～200 MHz分析频率内，当入射光功率减小为原来的1/2时，散粒噪声功率降低约3 dB，说明探测器的交流输出端在1～8 mW入射光功率范围内，具备良好的线性增益特性。在分析频率小于10 kHz处，当光功率为1 mW时，由于探测器电子学噪声迅速增加，信噪比较低，故测量的散粒噪声信号存在一定误差。

基于基尔霍夫电流定律的“自减”设计避免了放大器件不对称造成的共模抑制比下降。然而，不同光电二极管的响应曲线存在差异，故还需要补偿不同光电二极管的幅度特性和相位特性[20]。由于50/50光学分束器的分束比和光电二极管量子效率并不完全对称，故将分束器的输出端跳线绕制成一定圈数的光纤线圈，通过挤压光纤线圈改变线圈的半径，以精密调节光纤的衰减使光电流强度平衡，从而补偿光电二极管幅度特性差异，提高探测器的共模抑制比。光电二极管的相位特性主要由结电容决定，调节加载到光电二极管的反向偏置电压来改变结电容，实现光电二极管相位特性的精确调节，从而进一步提高探测器的共模抑制比。在测试平衡零拍探测器的共模抑制比时，信号

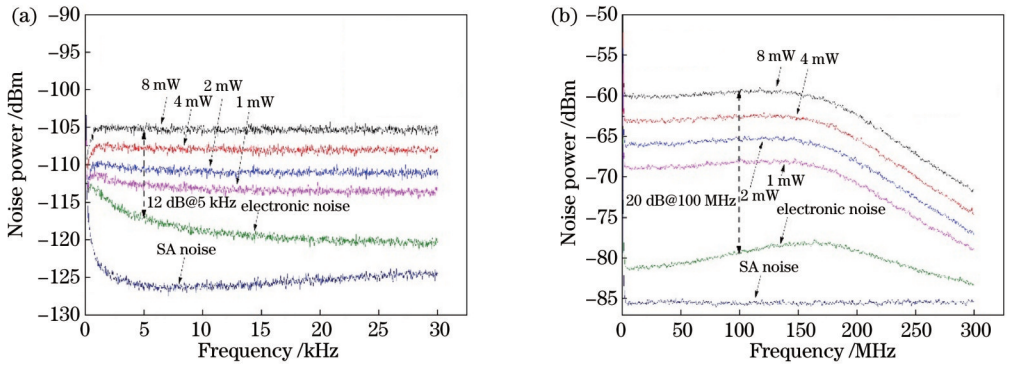

图 4 不同入射光功率下的散粒噪声功率、探测器噪声功率和频谱分析仪噪声功率。(a)低频段(0～30 kHz);(b)高频段(30 kHz～200 MHz)

Fig. 4 Shot noise powers under different incident optical powers, detector noise power, and spectrum analyzer noise power. (a) Low frequency band (0-30 kHz); (b) high frequency band (30 kHz-200 MHz)

发生器分别产生频率为 5 kHz 和 100 MHz 的正弦信号加载到电光振幅调制器上对激光的强度噪声进行调制。测试结果如图 5 所示,图 5(a)中的曲线对应探测器处于非平衡状态下的共模信号功率(挡住一个光电二极管,另一个光电二极管注入功率为 2 mW 的激光)、探测器处于平衡状态下的差模信号功率(两个光电二极管均注入功率为 2 mW 的激光)、探测器的电子学噪声功率和频谱分析仪的背景噪声功率。在 5 kHz 分析频率处,共模抑制比可达到 70 dB,探测器对共模输入噪声有良好的抑制作用。图 5(b)中的曲线分别对应探测器处于非平衡状态下的共模信号功率(挡住一个光电二极管,另一个光电二极管注入功率为 0.55 mW 的激光)、探测器处于平衡状态下的差模信号功率(两个光电二极管均注入功率为 0.55 mW 的激光)、探测器的电子学噪声功率和频谱分析仪的背景噪声功率。在 100 MHz 分析频率处,共模抑制比可达到 66 dB。

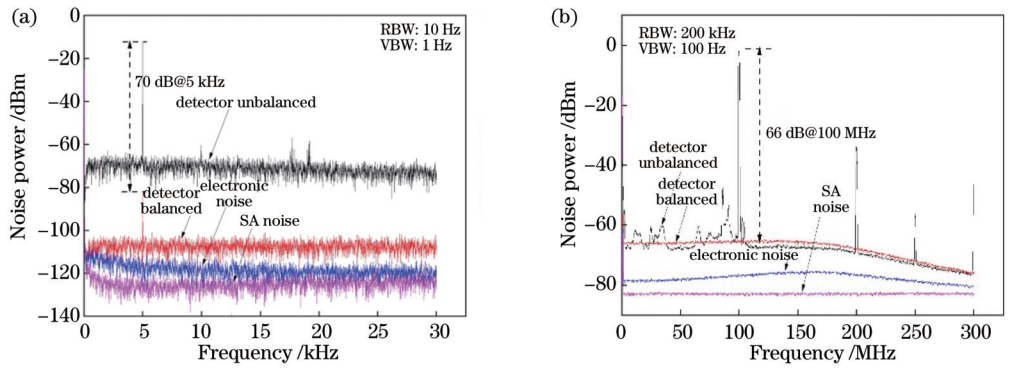

图 5 探测器共模抑制比测试结果。(a)低频段(0～30 kHz);(b)高频段(30 kHz～200 MHz)

Fig. 5 Test result of common mode rejection ratio of detector. (a) Low frequency band (0-30 kHz); (b) high frequency band (30 kHz-200 MHz)

4 结 论

基于平衡零拍探测器的等效噪声模型,理论分析了探测器的噪声来源。在理论指导下,合理选择元器件并采用 R-C 耦合结构,可以避免电感引入的不良效应。研制的宽带平衡零拍探测器在千赫兹分析频率处的电子学噪声相较 L-C 耦合结构[19]得到显著降低,并通过降低电路的寄生效应将工作带宽提升至 200 MHz。当光功率为 8 mW 的 1550 nm 激光入射时,5 kHz 分析频率处的信噪比为 12 dB,而 100 MHz 分析频率处的信噪比可达到 20 dB。同时,该探测器在低频和高频处均具有良好的共模抑制比和线性增益特性。所设计探测器为低频引力波探测、高速连续变量量子密钥分发和高速量子随机数发生器等应用提供了高性能的探测工具。

参 考 文 献

[1] Yuen H P, Chan V W. Noise in homodyne and heterodyne detection[J]. Optics Letters, 1983, 8(3): 177-179.

[2] Lvovsky A I, Raymer M G. Continuous-variable optical quantum-state tomography[J]. Reviews of Modern Physics, 2009, 81(1): 299-332.

[3] Leonhardt U. Measuring the quantum state of light[J]. Measurement Science and Technology, 2000, 11(12): 1827-1828.

[4] Wang S F, Xiang X, Zhou C H, et al. Sub-shot-noise interferometric timing measurement with a squeezed frequency

comb[J]. Physical Review A, 2018, 98(5): 053821.
[5] Zhou H J, Yang W H, Li Z X, et al. A bootstrapped, low-noise, and high-gain photodetector for shot noise measurement [J]. Review of Scientific Instruments, 2014, 85(1): 013111.
[6] Grote H, Weinert M, Adhikari R X, et al. High power and ultra-low-noise photodetector for squeezed-light enhanced gravitational wave detectors[J]. Optics Express, 2016, 24(18): 20107-20118.
[7] Khalaidovski A, Vahlbruch H, Lastzka N, et al. Long-term stable squeezed vacuum state of light for gravitational wave detectors[J]. Classical and Quantum Gravity, 2012, 29(7): 075001.
[8] Chi Y M, Qi B, Zhu W, et al. A balanced homodyne detector for high-rate Gaussian-modulated coherent-state quantum key distribution[J]. New Journal of Physics, 2011, 13(1): 013003.
[9] Ma X C, Sun S H, Jiang M S, et al. Enhancement of the security of a practical continuous-variable quantum-key-distribution system by manipulating the intensity of the local oscillator[J]. Physical Review A, 2014, 89(3): 032310.
[10] Ivanova A E, Chivilikhin S A, Popov I Y, et al. On the possibility of using optical Y-splitter in quantum random number generation systems based on fluctuations of vacuum[J]. Nanosystems: Physics, Chemistry, Mathematics, 2015, 6(1): 95-99.
[11] 魏世海, 樊矾, 杨杰, 等. 高速小型化光量子随机数发生器[J]. 中国激光, 2018, 45(5): 0512001.
Wei S H, Fan F, Yang J, et al. Ultrafast compact optical quantum random number generator[J]. Chinese Journal of Lasers, 2018, 45(5): 0512001.
[12] 王少锋, 项晓, 董瑞芳, 等. 量子光频梳产生实验研究[J]. 光学学报, 2018, 38(10): 1027003.
Wang S F, Xiang X, Dong R F, et al. Research on experimental generation of quantum optical frequency comb[J]. Acta Optica Sinica, 2018, 38(10): 1027003.
[13] 彭堃墀, 贾晓军, 苏晓龙, 等. 连续变量量子态的光学操控[J]. 光学学报, 2011, 31(9): 0900107.
Peng K C, Jia X J, Su X L, et al. Optical manipulations of quantum states with continuous variables[J]. Acta Optica Sinica, 2011, 31(9): 0900107.
[14] 周倩倩, 刘建丽, 张宽收. 量子光学实验中宽带低噪声光电探测器的研制[J]. 量子光学学报, 2010, 16(2): 152-157.
Zhou Q Q, Liu J L, Zhang K S. Low-noise, broadband photo-detector designs in quantum optics[J]. Acta Sinica Quantum Optica, 2010, 16(2): 152-157.
[15] Kumar R, Barrios E, Macrae A, et al. Versatile wideband balanced detector for quantum optical homodyne tomography[J]. Optics Communications, 2012, 285(24): 5259-5267.
[16] Huang D, Fang J, Wang C, et al. A 300-MHz bandwidth balanced homodyne detector for continuous variable quantum key distribution[J]. Chinese Physics Letters, 2013, 30(11): 468-477.
[17] Zhang X X, Zhang Y C, Li Z Y, et al. 1.2-GHz balanced homodyne detector for continuous-variable quantum information technology[J]. IEEE Photonics Journal, 2018, 10(5): 6803810.
[18] Wang J R, Wang Q W, Tian L, et al. A low-noise, high-SNR balanced homodyne detector for the bright squeezed state measurement in 1-100 kHz range[J]. Chinese Physics B, 2020, 29(3): 034205.
[19] 王少锋, 董瑞芳, 刘涛, 等. L-C 耦合电路对散粒噪声探测器电子学噪声的影响[J]. 光子学报, 2017, 46(7): 0704001.
Wang S F, Dong R F, Liu T, et al. Effect of L-C combination circuit on electronic noise of shot noise photodetector[J]. Acta Photonica Sinica, 2017, 46(7): 0704001.
[20] Jin X L, Su J, Zheng Y H, et al. Balanced homodyne detection with high common mode rejection ratio based on parameter compensation of two arbitrary photodiodes[J]. Optics Express, 2015, 23(18): 23859-23866.
[21] 王金晶, 贾晓军, 彭堃墀. 平衡零拍探测器的改进[J]. 光学学报, 2012, 32(1): 0127001.
Wang J J, Jia X J, Peng K C. Improvement of balanced homodyne detector[J]. Acta Optica Sinica, 2012, 32(1): 0127001.
[22] Johnson M. Photodetection and measurement: maximizing performance in optical systems[M]. New York: McGraw-Hill, 2003: 45-62.
[23] Wang S F, Xiang X, Zhou C H, et al. Simulation of high SNR photodetector with L-C coupling and transimpedance amplifier circuit and its verification[J]. Review of Scientific Instruments, 2017, 88(1): 013107.
[24] Graeme J G. Photodiode amplifiers: op amp solutions[M]. Boston: McGraw Hill, 1996: 87-90.
[25] 张正茂, 陈峰. 光电探测放大器的噪声分析[J]. 光电技术应用, 2012, 27(3): 37-40.
Zhang Z M, Chen F. Noise analysis of opto-electronic detection amplifier[J]. Electro-Optic Technology Application, 2012, 27(3): 37-40.

Design of 1 kHz-200 MHz Broadband Balanced Homodyne Detector Based on R-C Coupled Circuit

Wang Shaofeng[1,2**], Liu Xuanze[2], Li Hanqing[2], Li Kangkang[2], Dong Ruifang[1*]

[1]*Key Laboratory of Time and Frequency Primary Standards, National Time Service Center, Chinese Academy of Sciences, Xi'an* 710600, *Shaanxi, China*;

[2]*College of Physics and Electronic Engineering, Shanxi University, Taiyuan* 030006, *Shanxi, China*

Abstract

Objective The balanced homodyne detector (BHD) is widely used in quantum noise measurement, gravitational wave detection, high-sensitivity interferometric timing measurement, continuous-variable quantum key distribution, and quantum random number generation. Highly sensitive to the amplitude and phase of the incident light, the BHD can reliably extract quantum fluctuations, suppress the classical common-mode noise, and amplify quantum fluctuations to the macro level. However, the performance of the BHD is limited by the bandwidth, signal-to-noise ratio (SNR), and

common-mode rejection ratio (CMRR) of the detector. The optimal design of the BHD has always been a research hotspot. The transimpedance circuit based on a direct current (DC) coupled circuit is not suitable for detecting quantum noise. The reason is that as the power of the incident light increases, the unbalanced DC increases rapidly, and the transimpedance amplifier is saturated, which significantly reduces the dynamic range of the BHD. The BHD based on an inductor-capacitor (L-C) coupled circuit generates higher electronic noise at an analyzing frequency in the kHz range. It is not suitable for low-frequency measurements due to the parasitic effect of the inductor and the low impedance of the inductor at an analyzing frequency in the kHz range. In this paper, the noise sources of the BHD are analyzed theoretically, and a resistor-capacitor (R-C) coupled transimpedance circuit is used to improve the performance of the BHD at an analyzing frequency in the kHz range. Furthermore, the transimpedance circuit is optimized to increase the bandwidth to 200 MHz. The CMRR of the BHD is improved by designing a self-subtraction photodetector scheme, a variable optical attenuator, and an adjustable reverse bias voltage. These designs allow the BHD to meet the low-frequency and high-frequency measurements with high SNR and CMRR in quantum noise measurement.

Methods To enable the BHD to measure both low-frequency and high-frequency signals with high sensitivity, this paper adopts the BHD based on an R-C coupled transimpedance circuit. Two photodiodes are connected in series, and the balanced current signal in the two photodiodes is divided into a DC signal and an alternating current (AC) signal by the R-C coupled structure. The AC signal is converted into a voltage signal by a transimpedance amplifier (TIA) and is further used to measure the shot-noise power of the incident light. The DC signal is converted into a voltage signal by a load resistor and is then used to measure the balance between the two incident lights. To reduce the crosstalk between the DC circuit and the AC circuit, an isolation amplifier is added after the load resistor. An adjustable bias voltage (BV) circuit is used to adjust the junction capacitance of the photodiodes and further improve the CMRR. To compensate for the difference in the amplitude of the two photodiodes and thereby improve the CMRR of the BHD, the paper also utilizes a variable optical attenuator based on fiber bending, where variable attenuation is achieved by changing the radius of the bent fiber. The attenuation of the fiber is precisely adjusted to balance the photocurrent. In addition, an equivalent noise model is constructed. The electronic noise from the TIA circuit includes four parts, i. e., the noise introduced by the dark current in the photodiodes, the thermal noise in the feedback resistor, the noise generated by the input current noise in the TIA, and the noise produced by the input voltage noise. On the basis of theoretical analysis, reasonable DC load resistance and feedback capacitance, photodiodes with low dark current and low junction capacitance, and a TIA with low input noise are selected to reduce the electronic noise and improve the SNR of the BHD.

Results and Discussions A BHD with an R-C coupled circuit structure is designed (Fig. 1). A test device is built to test the performance of the BHD. The AC output is connected with a spectrometer to measure the bandwidth and the SNR of the BHD. The DC output is connected with an oscilloscope to make sure that the power of the two incident lights is balanced (Fig. 3). When the incident optical power is 8, 4, 2, and 1 mW, respectively, the paper tests the shot-noise spectrum and the electronic noise spectrum of the BHD with different analyzing frequencies. The test results show that the 3-dB bandwidth of the BHD is 1 kHz–200 MHz. The resolution bandwidth (RBW) and the video bandwidth (VBW) of the spectrum analyzer are set to 10 Hz and 1 Hz, respectively, and the number of averaging times is set to 40. In this case, the SNR is 12 dB at the analyzing frequency of 5 kHz under an incident optical power of 8 mW. The SNR is 20 dB at the analyzing frequency of 100 MHz when the RBW is 200 kHz and the VBW is 100 Hz. Moreover, in the analyzing frequency range of 10 kHz–200 MHz, the shot-noise power decreases by about 3 dB when the incident optical power decreases by half, indicating that the AC output of the BHD has favorable linear gain characteristics in the range of 1 mW to 8 mW (Fig. 4). In addition, 5 kHz and 100 MHz sinusoidal signals are loaded into an electro-optical amplitude modulator to modulate the incident light and thereby test the CMRR. The results show that the CMRR is 70 dB at the analyzing frequency of 5 kHz and 66 dB at the analyzing frequency of 100 MHz (Fig. 5).

Conclusions By analyzing the noise sources of the BHD, adopting the R-C coupled transimpedance circuit, and optimizing the TIA circuit, this paper implements a broadband balanced homodyne detector that works in the bandwidth range from 1 kHz to 200 MHz with low noise and high CMRR. In the case of an incident optical power of 8 mW@1550 nm, the shot-noise power is 12 dB higher than the electronic noise power and the CMRR reaches 70 dB at the analyzing frequency of 5 kHz, and the shot-noise power is 20 dB higher than the electronic noise power and the CMRR reaches 66 dB at the analyzing frequency of 100 MHz. Such a homodyne detector can serve as a high-performance detection tool in various applications, such as low-frequency gravitational wave detection, high-speed continuous-variable quantum key distribution, and high-speed quantum random number generation.

Key words optical devices; transimpedance amplifier; shot noise; common-mode rejection ratio; signal-to-noise ratio; electronic noise